Transition Met Chem (2016) 41:375–385
DOI 10.1007/s11243-016-0033-8

Hydrothermal syntheses and photocatalytic performance of three Mn-based coordination complexes constructed from 1,10-phenanthroline and polycarboxylic acids

Chong-Chen Wang[1,2] · Fang Gao[1] · Xin-Xing Guo[1] · Huan-Ping Jing[1] · Peng Wang[1] · Shi-Jie Gao[1]

Received: 8 December 2015 / Accepted: 12 February 2016 / Published online: 26 February 2016

Abstract Three coordination complexes based on manganese, namely Mn(phen)(5-Br-ipa) (**1**), Mn(phen)(5-NO_2-ipa) (**2**), and [Mn(phen)$_2$(3,4-H_2dczpb)]·H_2O (**3**) (phen = 1,10-phenanthroline; 5-Br-ipa = 5-bromoisophthalic acid; 5-NO_2-ipa = 5-nitroisophthalic acid; 3,4-H_4dczpb = 3,4-dicarboxyl-(3′,4′-dicarboxylazophenyl)benzene), have been synthesized under hydrothermal conditions and characterized by single-crystal X-ray diffraction, FTIR, elemental analysis, and UV–Vis diffuse reflection spectroscopy. The photocatalytic efficiencies of the complexes for the decomposition of methylene blue under UV irradiation were also investigated. These complexes show 2D sheet, 1D chain and 0D discrete structures due to the different coordination environments of the Mn(II) centers and the number of phen ligands.

Introduction

In view of their diverse and easily tailored structures, along with their various potential applications in catalysis and photocatalysis [1, 2], separation [3], gas storage [4], carbon dioxide capture [5] and so on [6, 7], functional inorganic–organic hybrid porous materials constructed from coordination complexes have gained continuing attention [6, 8]. Most recently, such coordination complexes have been found to have potential as heterogeneous photocatalysts due to the presence of catalytically active metals and/or functional organic linkers as well as easily tailorable physical and chemical functions and catalytic properties [9]. In recent years, much attention has been given to the use of such complexes for the degradation of organic pollutants [10–12], CO_2 reduction [13, 14] and water splitting [15, 16].

The construction of such coordination complexes is influenced by many factors including but not limited to the types of metal atoms, organic ligands, solvents, and counter-ions [10, 17]. In particular, the alteration of the organic ligands can lead to very different structures [18, 19]. As bridging ligands, carboxylates, especially multicarboxylates, are of immense interest in the construction of coordination architectures owing to the fact that the resulting complexes have a wide range of structural diversities and potential applications as porous materials [17, 20, 21]. In recent years, rigid 5-R-isophthalic acids (5-R-H_2ipa, R = –OH, –CH_3, –Br, –OCH_3, –NO_2) have been used for the preparation of various coordination compounds [22–26]. In order to investigate the influence of functional groups attached to the ipa ligand on the structure of the resulting coordination complexes, in this paper, three different multicarboxylic acid ligands, namely 5-bromoisophthalic acid (5-Br-ipa), 5-nitroisophthalic acid (5-NO_2-ipa), and 3,4-dicarboxyl-(3′,4′-dicarboxylazophenyl) benzene (3,4-H_4dczpb) (Scheme 1) along with 1,10-phenanthroline (phen) as a terminal chelating ligand were utilized to build three novel manganese(II) coordination complexes with different structures, formulated as Mn(phen)(5-Br-ipa) (**1**), Mn(phen)(5-NO_2-ipa) (**2**), and [Mn(phen)$_2$(3,4-H_2dczpb)]·H_2O (**3**). The crystal structures of the complexes, as well as their optical gaps and

✉ Chong-Chen Wang
chongchenwang@126.com

[1] Key Laboratory of Urban Stormwater System and Water Environment (Ministry of Education), Beijing 100044, China

[2] Beijing Engineering Research Center of Sustainable Urban Sewage System Construction and Risk Control, Beijing University of Civil Engineering and Architecture, Beijing 100044, China

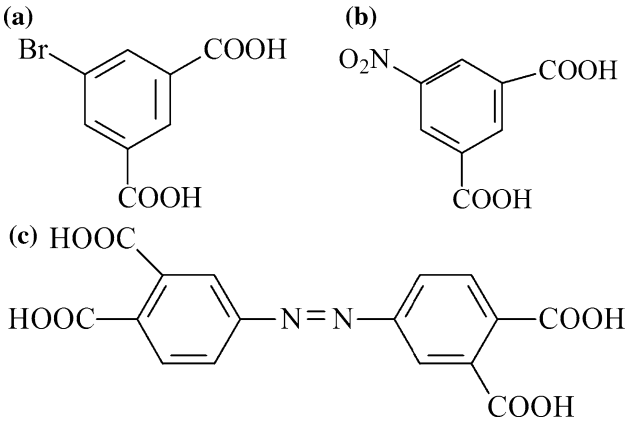

Scheme 1 Structural formulae of 5-Br-ipa (**a**), 5-NO_2-ipa (**b**) and 3,4-H_4dczpb (**c**)

photocatalytic activities toward the degradation of methylene blue (MB), have been investigated.

Experimental

Materials and methods

All chemicals were commercially available reagent grade and used without further purification. CNH elemental analyses were obtained using an Elementar Vario EL-III instrument. The FTIR spectra, in the region (400–4000 cm^{-1}), were recorded on a Nicolet 6700 Fourier Transform infrared spectrophotometer. UV–Vis diffuse reflection spectroscopy (DRS) of solid samples were measured from 200 to 1200 nm with a PerkinElmer Lamda 650S spectrophotometer using $BaSO_4$ was used as the standard with 100 % reflectance.

*Synthesis of Mn(phen)(5-Br-ipa) (**1**)*

A mixture of $MnCl_2{\cdot}4H_2O$ (0.0594 g, 0.3 mmol), 5-Br-H_2ipa (0.0735 g, 0.3 mmol) and 1,10-phen (0.1189 g, 0.6 mmol) was sealed in a 25 mL Teflon-lined stainless steel Parr bomb containing deionized H_2O (20 mL), heated at 160 °C for 72 h, and then cooled down to room temperature. Small yellow rod-like crystals of complex **1** (yield 90 % based on $MnCl_2{\cdot}4H_2O$) were isolated and washed with deionized water and ethanol. Anal. Calcd. for **1**, $C_{20}H_{11}BrMnN_2O_4$: C, 50.2; N, 5.9; H, 2.3. Found: C, 50.3; N, 5.9; H, 2.4 %. IR (KBr)/cm^{-1}: 3417m, 3089m, 1619s, 1567m, 1530m, 1518m, 1451m, 1426s, 1344m, 1145w, 1102w, 920m, 865m, 852m, 790m, 730m, 639m, 537w, 421w.

*Synthesis of Mn(phen)(5-NO_2-ipa) (**2**)*

Yellow block-like crystals of **2** (yield 61 % based on $MnCl_2{\cdot}4H_2O$) were synthesized from a mixture of $MnCl_2{\cdot}4H_2O$ (0.0594 g, 0.3 mmol), 5-NO_2-H_2ipa (0.0663 g, 0.3 mmol) and 1,10-phen (0.1189 g, 0.6 mmol) under the same conditions as complex **1**. Anal. Calcd. for **2**, $C_{20}H_{11}MnN_3O_6$: C, 54.0; N, 6.3; H, 2.5. Found: C, 54.2; N, 6.2; H, 2.7 %. IR (KBr)/cm^{-1}: 3417m, 3091m, 1607s, 1573m, 1532m, 1425s, 1375m, 1351m, 1140w, 1102w, 1078m, 922m, 843m, 789m, 731m, 640m, 545w, 421w.

*Synthesis of [Mn(phen)$_2$(3,4-H_2dczpb)]·H_2O (**3**)*

Yellow block-like crystals of **3** (yield 40 % based on $MnCl_2{\cdot}4H_2O$) were synthesized from a mixture of $MnCl_2{\cdot}4H_2O$ (0.0594 g, 0.3 mmol), 3,4-H_2dczpb (0.1074 g, 0.3 mmol) and 1,10-phen (0.1189 g, 0.6 mmol) in 1:1:2 M ratio under the same conditions as complex **1**. Anal. Calcd. for **3**, $C_{40}H_{26}MnN_6O_9$: C, 60.8; N, 10.6; H, 3.3. Found: C, 60.9; N, 10.5; H, 3.5 %. IR (KBr)/cm^{-1}: 3449m, 3047m, 1938m, 1694m, 1589m, 1517s, 1427s, 1375m, 1261m, 1101w, 1049m, 865m, 845m, 789m, 776m, 727m, 655m, 638m, 515w, 420w.

X-ray crystallography

X-ray single-crystal data collection for the complexes **1–3** was performed with Bruker Smart 1000 CCD area detector diffractometer with graphite-monochromatized MoKα radiation ($\lambda = 0.71073$ Å) using φ–ω mode at 293(2) K. The SMART software [27] was used for data collection and SAINT software [27] for data extraction. Empirical absorption corrections were performed with the SADABS program [28]. The structures were solved by direct methods (SHELXS-97) [29] and refined by full-matrix-least squares techniques on F^2 with anisotropic thermal parameters for all of the non-hydrogen atoms (SHELXL-97) [29]. The hydrogen atoms of the organic ligands were added according to theoretical models, and those of water molecules were found by difference Fourier maps. All structural calculations were carried out using the SHELX-97 program package [29]. Crystallographic data and structural refinements for the complexes **1–3** are summarized in Table 1. Selected bond lengths and angles for both compounds are listed in Table 2.

Photocatalytic degradation of MB

The activities of complexes **1–3** as photocatalysts were evaluated via degradation of MB at room temperature under 500 W Hg lamp irradiation in a photocatalytic assessment system (Beijing Aulight Co. Ltd.). The distance between the light source and the beaker containing reaction mixture was fixed at 5 cm. The solid photocatalyst (50 mg) was added to 200 mL of MB (10 mg/L) aqueous solution in a 300-mL beaker. Prior to irradiation, the suspension was magnetically stirred in the dark for 120 min to ensure

Table 1 Details of X-ray data collection and refinement for compounds **1–3**

	1	**2**	**3**
Formula	$C_{20}H_{11}BrMnN_2O_4$	$C_{20}H_{11}MnN_3O_6$	$C_{40}H_{26}MnN_6O_9$
M	478.16	444.26	789.61
Crystal system	Monoclinic	Triclinic	Monoclinic
space group	P2(1)/n	Pī	P2(1)/c
a (Å)	10.1641(8)	10.0570(9)	14.8740(13)
b (Å)	14.4226(15)	14.3339(12)	20.7329(19)
c (Å)	24.659(2)	14.6521(13)	12.1094(11)
α (°)	90	104.0510(10)	90
β (°)	94.5260(10)	102.6170(10)	110.758(2)
γ (°)	90	110.478(2)	90
V (Å^3)	3603.6(6)	1809.4(3)	3491.9(5)
Z	8	4	4
μ(Mo, Kα) (mm^{-1})	2.981	0.776	0.447
Total reflections	17,278	9141	17,607
Unique	6315	6263	6168
F(000)	1896	900	1620
Goodness-of-fit on F^2	1.005	1.028	1.068
R_{int}	0.1011	0.0477	0.0658
*R*1	0.0526	0.0752	0.0838
ω*R*2	0.1002	0.1879	0.2010
*R*1 (all data)	0.0911	0.1366	0.1177
ω*R*2 (all data)	0.1110	0.2231	0.2135
Largest diff. Peak and hole (e/Å^3)	0.757, −0.923	1.313, −0.402	0.464, −0.375

the establishment of an adsorption/desorption equilibrium. During the photocatalytic degradation reaction, stirring was maintained to keep the mixture in complete suspension. Aliquots of volume 1 ml were extracted at regular intervals using a 0.45-μm syringe filter (Shanghai Troody) for analysis. A Laspec Alpha-1860 spectrometer was used to monitor the changes in dye absorbance in the range of 400–800 nm in a spectrometric quartz cell with 1 cm path length. The MB concentration was determined from its maximum absorbance at 664 nm.

Results and discussion

Structures of the complexes

All these three complexes are stable in water and common organic solvents like methanol, alcohol, ether, *N*,*N*-dimethylformamide, and so on.

Mn(phen)(5-Br-ipa) (**1**) was synthesized under hydrothermal conditions. The crystal structure analysis reveals that complex **1** is built up of 2D neutral Mn(phen)(5-Br-ipa) sheets, as illustrated in Fig. 1b. The nearly identical Mn1 and Mn2 centers, in an octahedral geometry, are each six-coordinated by two nitrogen atoms from a phen ligand, two oxygen atoms from two different monodentate 5-Br-ipa^{2-} ligands, and two oxygen atoms from a chelating 5-Br-ipa^{2-} ligand. Taking Mn1 as an example, N1 and O5 occupy the axial positions, and the remaining atoms N2, O1, O3 and O4 atoms lie in the four sites of the equatorial plane of Mn1, as depicted in Fig. 1a. In the equatorial plane, the N2–Mn1–O3$^{\#1}$, O1–Mn1–O4$^{\#1}$, O3$^{\#1}$–Mn1–O4$^{\#1}$, and O1–Mn1–N2 bond angles are 150.37(13), 92.95(13), 57.82(13), and 114.35(13)°, respectively, and the N1–Mn1–O5 bond angle is 161.22(14)°, implying that the Mn-centered coordination octahedron is seriously distorted. The Mn–O and Mn–N bond distances compare with the normal values for these bonds as found in similar CPs [17].

The 5-Br-H_2ipa ligand has often been adopted as a component for building coordination compounds with or without auxiliary ligands, as it is a kind of polydentate ligand which may act as a linker with different geometric effects to connect metal centers into multidimensional structures via various coordination modes [30–35]. In complex **1**, the completely deprotonated 5-Br-ipa^{2-} acts as a tridentate ligand, joining Mn(II) centers via both chelating and bis-mono modes to form two-dimensional Mn(5-Br-ipa) sheets modified by phen ligands, as illustrated in Fig. 1b–d and Scheme 2a. The 2D Mn(phen)(5-Br-ipa) sheets are further linked into a three-dimensional structure via π-π stacking interactions, as listed in Table 4.

Table 2 Selected bond lengths (Å) and angles (°) for compound **1–3**

(**1**)					
Bond lengths (Å)					
Mn(1)-O(5)	2.143(3)	Mn(1)-O(1)	2.169(3)	Mn(1)-O(3)#1	2.249(4)
Mn(1)-N(1)	2.263(4)	Mn(1)-O(4)#1	2.296(3)	Mn(1)-N(2)	2.322(4)
Mn(2)-O(6)	2.083(3)	Mn(2)-O(2)	2.122(4)	Mn(2)-O(7)	2.247(3)
Mn(2)-N(4)	2.260(4)	Mn(2)-O(8)	2.276(3)	Mn(2)-N(3)	2.306(4)
Bond angles (°)					
O(5)-Mn(1)-O(1)	101.56(13)	O(5)-Mn(1)-O(3)#1	106.10(12)		
O(1)-Mn(1)-O(3)#1	86.39(13)	O(5)-Mn(1)-N(1)	161.22(15)		
O(1)-Mn(1)-N(1)	81.05(13)	O(3)#1-Mn(1)-N(1)	92.60(14)		
O(5)-Mn(1)-O(4)#1	95.45(12)	O(1)-Mn(1)-O(4)#1	143.54(15)		
O(3)#1-Mn(1)-O(4)#1	57.82(13)	N(1)-Mn(1)-O(4)#1	92.95(13)		
O(5)-Mn(1)-N(2)	90.85(14)	O(1)-Mn(1)-N(2)	114.35(13)		
O(3)#1-Mn(1)-N(2)	150.37(13)	N(1)-Mn(1)-N(2)	71.42(15)		
O(4)#1-Mn(1)-N(2)	97.22(14)	O(6)-Mn(2)-O(2)	102.14(14)		
O(6)-Mn(2)-O(7)	93.96(12)	O(2)-Mn(2)-O(7)	100.36(13)		
O(6)-Mn(2)-N(4)	88.33(15)	O(2)-Mn(2)-N(4)	166.22(14)		
O(7)-Mn(2)-N(4)	87.66(14)	O(6)-Mn(2)-O(8)	150.64(13)		
O(2)-Mn(2)-O(8)	92.15(13)	O(7)-Mn(2)-O(8)	57.96(11)		
N(4)-Mn(2)-O(8)	82.57(14)	O(6)-Mn(2)-N(3)	122.46(13)		
O(2)-Mn(2)-N(3)	93.58(15)	O(7)-Mn(2)-N(3)	137.16(12)		
N(4)-Mn(2)-N(3)	73.09(15)	O(8)-Mn(2)-N(3)	81.40(12)		
Symmetry transformations used to generate equivalent atoms: #1 $-x + 3/2$, $y - 1/2$, $-z + 3/2$; #2 $-x + 3/2$, $y + 1/2$, $-z + 3/2$; #3 $-x + 1$, $-y + 1$, $-z + 1$					
(**2**)					
Bond lengths (Å)					
Mn(1)-O(1)	2.152(5)	Mn(1)-O(7)	2.164(5)	Mn(1)-O(10)#1	2.192(5)
Mn(1)-N(3)	2.243(6)	Mn(1)-N(4)	2.267(6)	Mn(1)-O(9)#1	2.372(5)
Mn(2)-O(2)	2.149(5)	Mn(2)-O(8)	2.156(5)	Mn(2)-N(6)	2.243(6)
Mn(2)-N(5)	2.251(6)	Mn(2)-O(3)#2	2.273(5)	Mn(2)-O(4)#2	2.278(5)
Bond angles (°)					
O(1)-Mn(1)-O(7)	97.82(19)	O(1)-Mn(1)-O(10)#1	98.72(19)		
O(7)-Mn(1)-O(10)#1	84.86(19)	O(1)-Mn(1)-N(3)	85.9(2)		
O(7)-Mn(1)-N(3)	130.8(2)	O(10)#1-Mn(1)-N(3)	143.4(2)		
O(1)-Mn(1)-N(4)	152.9(2)	O(7)-Mn(1)-N(4)		84.0(2)	
O(10)#1-Mn(1)-N(4)	108.4(2)	N(3)-Mn(1)-N(4)		73.0(2)	
O(1)-Mn(1)-O(9)#1	92.84(19)	O(7)-Mn(1)-O(9)#1	141.29(19)		
O(10)#1-Mn(1)-O(9)#1	56.70(18)	N(3)-Mn(1)-O(9)#1	86.91(19)		
N(4)-Mn(1)-O(9)#1	102.6(2)	O(2)-Mn(2)-O(8)		96.3(2)	
O(2)-Mn(2)-N(6)		85.4(2)	O(8)-Mn(2)-N(6)	158.9(2)	
O(2)-Mn(2)-N(5)	128.7(2)	O(8)-Mn(2)-N(5)		89.7(2)	
N(6)-Mn(2)-N(5)	73.2(2)	O(2)-Mn(2)-O(3)#2	141.78(19)		
O(8)-Mn(2)-O(3)#2	94.9(2)	N(6)-Mn(2)-O(3)#2	96.6(2)		
N(5)-Mn(2)-O(3)#2	87.67(19)	O(2)-Mn(2)-O(4)#2	85.00(18)		
O(8)-Mn(2)-O(4)#2	100.48(19)	N(6)-Mn(2)-O(4)#2	100.7(2)		
N(5)-Mn(2)-O(4)#2	143.74(19)	O(3)#2-Mn(2)-O(4)#2	57.03(17)		
Symmetry transformations used to generate equivalent atoms: #1 $x + 1$, y, z; #2 $x - 1$, y, z					
(**3**)					
Bond lengths (Å)					
Mn(1)-O(4)#1	2.099(4)	Mn(1)-O(3)	2.122(4)	Mn(1)-N(4)	2.257(5)

Table 2 continued

Mn(1)-N(1)	2.277(5)	Mn(1)-N(2)	2.299(5)	Mn(1)-N(3)	2.302(5)
Bond angles (°)					
O(4)#1-Mn(1)-O(3)	101.46(15)	O(4)#1-Mn(1)-N(4)	96.89(16)		
O(3)-Mn(1)-N(4)	91.96(17)	O(4)#1-Mn(1)-N(1)	94.90(17)		
O(3)-Mn(1)-N(1)	92.97(16)	N(4)-Mn(1)-N(1)	166.06(19)		
O(4)#1-Mn(1)-N(2)	165.26(18)	O(3)-Mn(1)-N(2)	86.46(16)		
N(4)-Mn(1)-N(2)	95.22(19)	N(1)-Mn(1)-N(2)	72.1(2)		
O(4)#1-Mn(1)-N(3)	88.93(16)	O(3)-Mn(1)-N(3)	162.15(18)		
N(4)-Mn(1)-N(3)	72.2(2)	N(1)-Mn(1)-N(3)	100.6(2)		
N(2)-Mn(1)-N(3)	86.79(17)				

Symmetry transformations used to generate equivalent atoms: #1 $-x + 1, -y + 1, -z + 1$

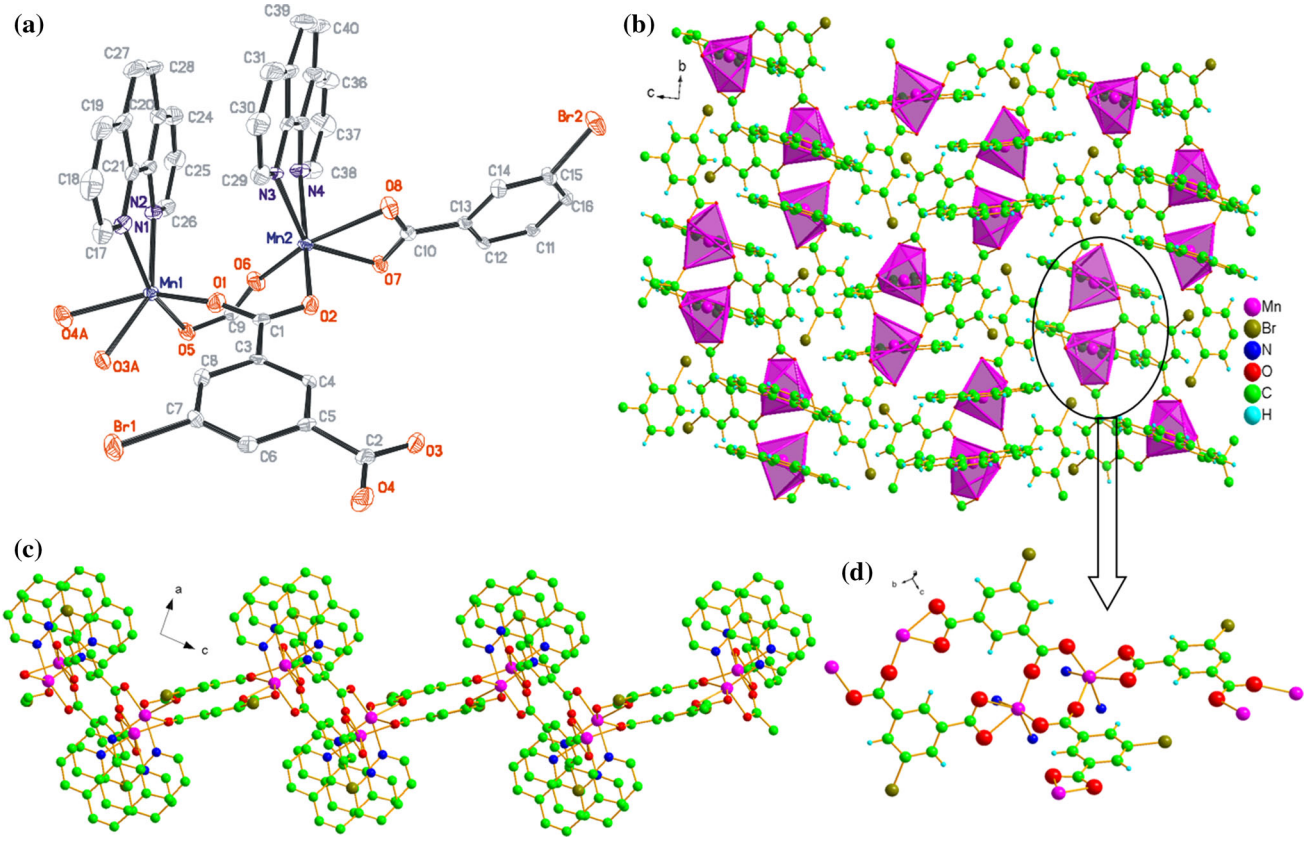

Fig. 1 **a** Asymmetric unit of Mn(phen)(5-Br-ipa) (**1**) and coordination environments around the Mn(II) atoms. **b** The 2D sheet of **1** viewed from *a*-axis. **c** 1D chains of **1** from *b*-axis. **d** The highlights of Mn(II) environment coordinated by phen and 5-Br-ipa ligand in **1** (H atoms are omitted for clarity)

Mn(phen)(5-NO_2-ipa) (**2**) was synthesized under identical conditions as **1**. Again, the Mn1 and Mn2 centers in **2**, are almost identical. For example, Mn1 is octahedrally coordinated by N3 and N4 from a phen ligand, O1 and O7 atoms from two different monodentate 5-NO_2-ipa^{2-} ligands, and O9 and O10 from one chelating 5-NO_2-ipa^{2-} ligand, as shown in Fig. 2a, b. The coordination environment of Mn(II) and coordination mode of the 5-NO_2-ipa^{2-} ligand in complex **2** are thus nearly identical with their counterparts in complex **1**. However, complexes 1 and 2 differ in possessing 1D chains as illustrated in Fig. 2c, d and Scheme 2b and 2D sheets as depicted in Fig. 1b,

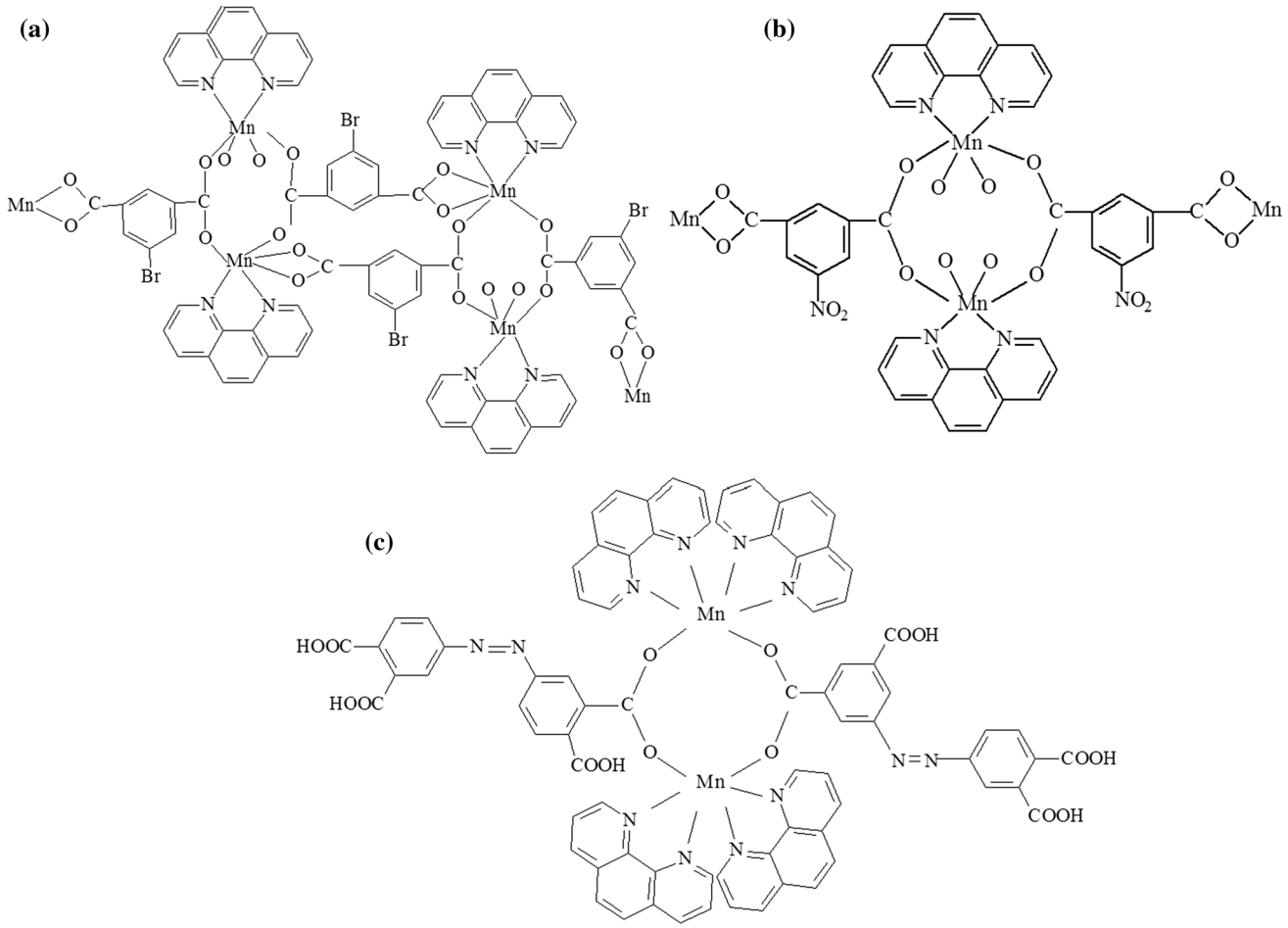

Scheme 2 Coordination environments of the Mn(II) centers in complexes **1–3**

respectively, which can be explained by the slight difference of O–Mn–O bond angles as listed in Table 2 and Scheme 2a, b. Finally, in complex 2, a three-dimensional supramolecular structure is built up of one-dimensional Mn(phen)(5-NO_2-ipa) chains via π–π stacking interactions as listed in Table 4.

The 3D supramolecular structure of [Mn(phen)$_2$(3,4-H_2dczpb)]·H_2O (**3**) is constructed from discrete zero-dimensional [Mn_2(phen)$_4$(3,4-H_2dczpb)] units and lattice water molecules via intermolecular hydrogen bonding interactions [O2-O5(x-1, y, z-1): 2.544 Å; O7-O6: 2.381 Å] (Fig. 3b, c; Table 3) and π–π stacking interactions as listed in Table 4. In the structure of complex **3**, Mn(II) is six-coordinated in a distorted octahedral geometry connected by four nitrogen atoms (N1, N2, N3 and N4) from two different phen ligands, plus two oxygen atoms (O3 and O4) from a bis-monodentate 3,4-H_2dczpb^{2-} ligand, as illustrated in Fig. 3a. The 3,4-H_2dczpb^{2-} anions acts as both bis-monodentate ligands to join two different Mn^{2+} centers and as counter-ions. The coordination mode of 3,4-H_2dczpb^{2-} in complex **3** is similar to that of the previously reported [Co_2(phen)$_4$(H_2dczpb)$_2$]·5H_2O [36], while being quite different from the [Mn_2(phen)$_4$(3,4-H_2dczpb)](3,4-H_4dczpb)$_2$·2H_2O [12]. The terminal COOH substituents on the other benzene ring of the 3,4-H_2dczpb^{2-} ligand and four coordination sites of Mn^{2+} being occupied by phen resulted in the low-dimensional structure of complex **3**.

Optical energy gap

To explore the conductivities of the complexes **1–3**, UV–Vis DRS was used on powder samples to obtain their corresponding band gap E_g [37, 38], determined as the intersection point between the energy axis and the line extrapolated from the linear portion of the absorption edge in a plot of Kubelka–Munk function F against energy E. The Kubelka–Munk function, $F = (1 - R)^2/2R$, was calculated from the recorded UV–Vis DRS data, where R is the reflectance of an infinitely thick layer at a given wavelength. The plots of F versus E for these complexes are shown in Fig. 4, where steep absorption edges are displayed. The E_g values were obtained as 2.9, 3.0 and

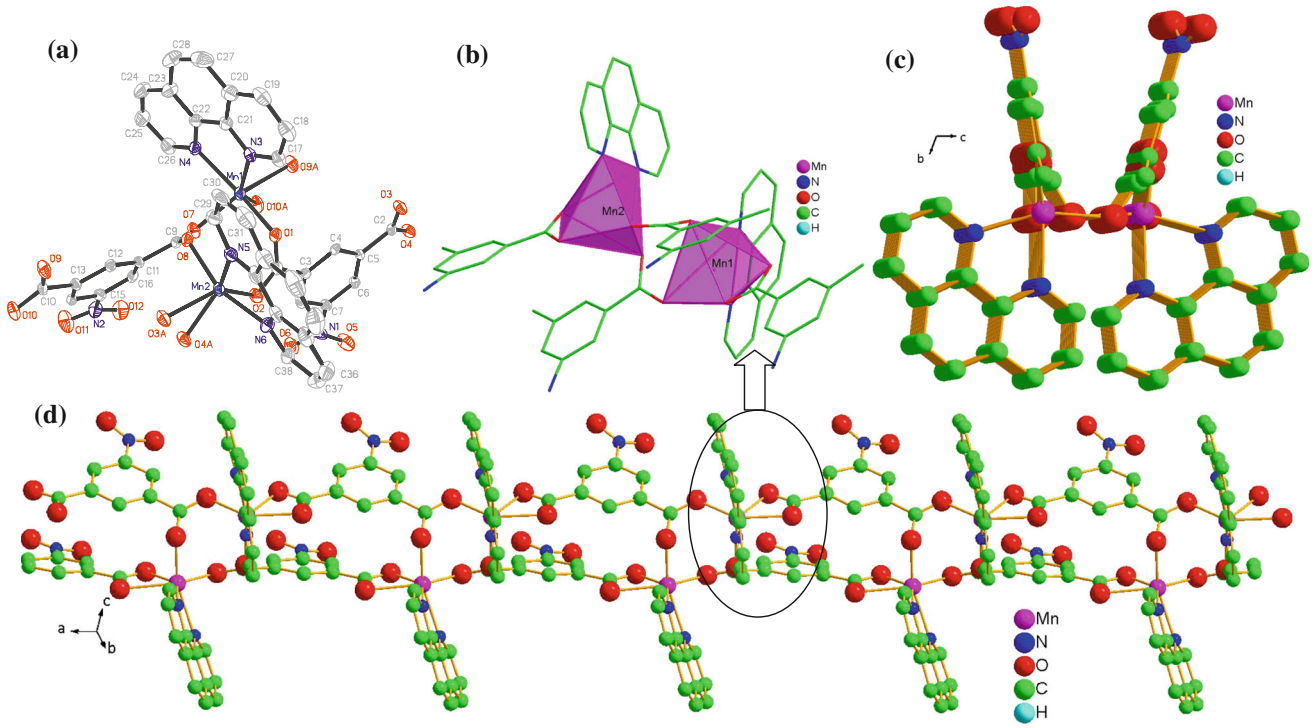

Fig. 2 **a** Asymmetric unit of Mn(phen)(5-NO_2-ipa) (**2**) and coordination environments around the Mn(II) atoms. **b** Highlight of the coordination environment of the Mn(II) centers**. c** Packing view of 1D chains from the *a*-axis. **d** 1D chain of compound **2**

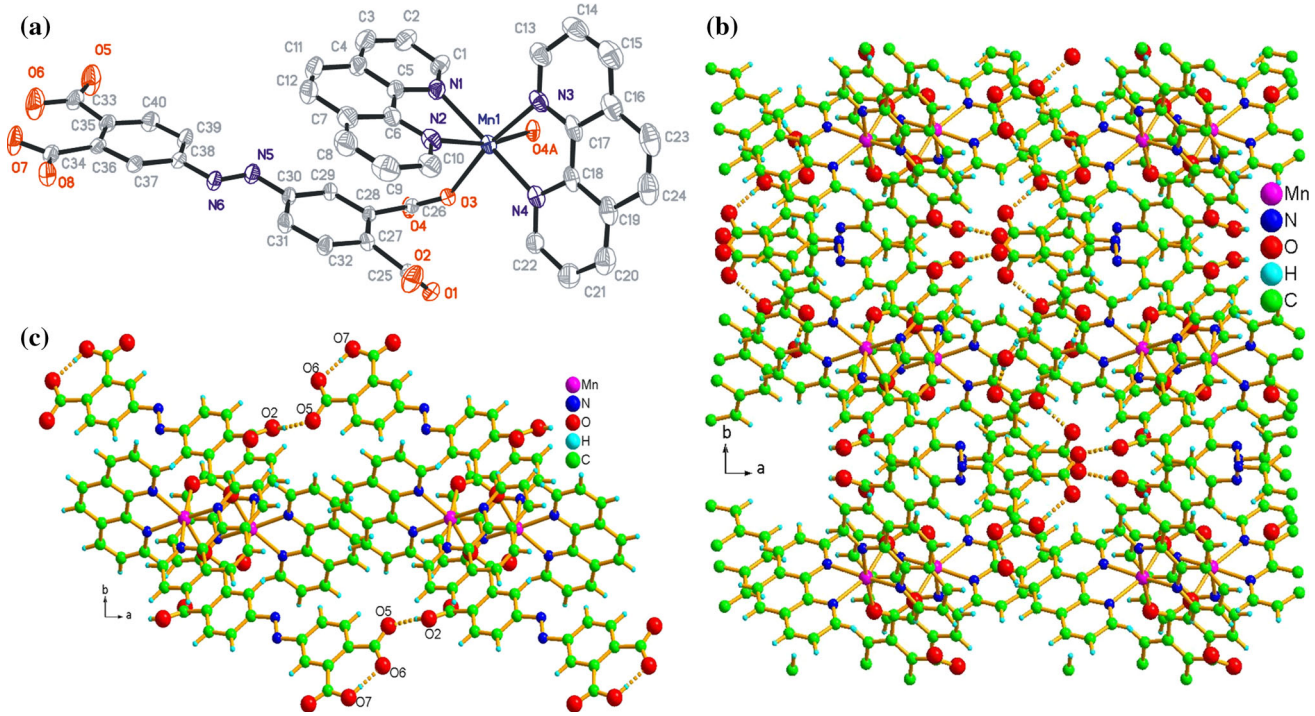

Fig. 3 **a** Ortep view of [Mn(phen)$_2$(3,4-H_2dczpb)]·H_2O (**3**). Lattice water molecules and H atoms are omitted for clarity. **b** 3D framework of **3** viewed along *c*-axis. **c** Hydrogen bonding interactions in the complex **3**

Table 3 Hydrogen bonds for compound **3** [Å and °]

D–H	d(D–H)	d(H…A)	<DHA	d(D..A)	A
O2–H2	0.820	1.741	166.16	2.544	O5 [x − 1, y, z − 1]
O7–H7	0.820	1.563	174.60	2.381	O6

Table 4 Defined ring and relative parameters of π-π interactions in compound **1–3**

Compound **1**

Cg(7): N(2) → C(22) → C(23) → C(24) → C(25) → C(26)→
Cg(8): N(3) → C(29) → C(30) → C(31) → C(32) → C(33)→
Cg(9): N(4) → C(34) → C(35) → C(36) → C(37) → C(38)→
Cg(12): C(20) → C(21) → C(22) → C(23) → C(28) → C(27)→

Cg(I) → Cg(J)	Dist. centroids (Å)	Dihedral angle (°)	Perp. Dist. (IJ) (Å)	Perp. Dist. (JI) (Å)
Cg(8) → Cg(12)	3.607(3)	4.9(2)	3.470(2)	3.484(2)
Cg(9) → Cg(7)	3.959(3)	5.5(2)	3.642(2)	3.478(2)

Compound **2**

Cg(9): N(5) → C(29) → C(30) → C(31) → C(32) → C(33)→
Cg(11): C(3) → C(4) → C(5) → C(6) → C(7) → C(8)→
Cg(12): C(11) → C(12) → C(13) → C(14) → C(15) → C(16)→

Cg(I) → Cg(J)	Dist. centroids (Å)	Dihedral angle (°)	Perp. Dist. (IJ) (Å)	Perp. Dist. (JI) (Å)
Cg(9) → Cg(9)^{i}	3.655(5)	0	3.319(4)	3.319(4)
Cg(11) → Cg(11)^{ii}	3.630(4)	0	3.340(3)	3.340(3)
Cg(12) → Cg(12)^{iii}	3.624(4)	0	3.354(3)	3.353(3)

Symmetry codes: (i) 1 − *x*, 2 − *y*, 1 − *z*; (ii) 2 − *x*, 1 − *y*, 1 − *z*; (iii) −*x*, 1 − *y*, −*z*

Compound **3**

Cg(4): N(2) → C(6) → C(7) → C(8) → C(9) → C(10)→
Cg(7): C(4) → C(5) → C(6) → C(7) → C(12) → C(11)→
Cg(8): C(16) → C(17) → C(18) → C(19) → C(24) → C(23)→
Cg(9): C(27) → C(28) → C(29) → C(30) → C(31) → C(32)→

Cg(I) → Cg(J)	Dist. centroids (Å)	Dihedral angle (°)	Perp. Dist. (IJ) (Å)	Perp. Dist. (JI) (Å)
Cg(4) → Cg(9)	3.642(4)	1.5(3)	3.444(3)	3.473(2)
Cg(9) → Cg(9)^{i}	3.554(5)	0	3.490(3)	3.490(3)
Cg(7) → Cg(9)	3.792(4)	2.7(3)	3.519(3)	3.450(2)
Cg(8) → Cg(8)^{ii}	3.773(5)	0	3.456(3)	3.456(3)
Cg(9) → Cg(4)	3.642(4)	0	3.473(2)	3.445(3)
Cg(7) → Cg(9)	3.792(4)	2.7(3)	3.450(2)	3.520(3)

Symmetry codes: (i) 1 − *x*, 1 − *y*, 2 − *z*; (ii) −*x*, 1 − *y*, 1 − *z*

3.2 eV for complexes **1**, **2** and **3**, respectively, implying that all three complexes show selective absorption in the visible and ultraviolet spectrum region [39, 40].

Photocatalytic studies

The photocatalytic performances of these complexes for the decomposition of MB were studied under UV irradiation. Control experiments on degradation of MB in the absence of catalysts were also performed. The photocatalytic performances were monitored by measuring the maximum absorbance intensity at $\lambda = 664$ nm to determine the residual concentration of MB. The degradation efficiencies of MB in the presence of complexes **1–3** after adsorption equilibrium in the dark are depicted in Fig. 5. All data are the average values of three parallel experiments. The degradation efficiency of

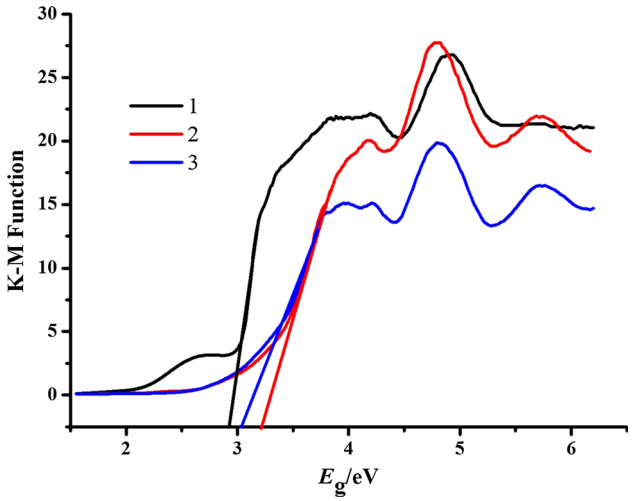

Fig. 4 Kubelka-Munk transformed diffuse reflectance spectra for complexes **1**–**3**

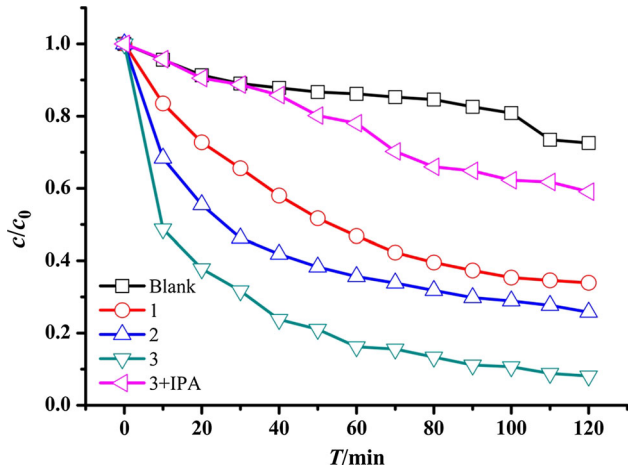

Fig. 5 *Plots* of concentration of MB versus irradiation time under irradiation with Hg lamp light with complexes **1**–**3** as photocatalysts, plus a control experiment without any photocatalyst

MB increased from 27.5 % (control experiment without any photocatalyst) to 66.1, 74.2 and 91.9 % with **1**, **2** and **3,** respectively, after 120 min. These photocatalytic degradation reactions each followed a pseudo-first-order kinetic model, with R^2 values of 0.949, 0.865 and 0.926 for **1**, **2** and **3**, respectively, evidenced by the linear plots of $-\ln(C/C_0)$ versus reaction time t, such that the pseudo-first-order rate constants (k) were 0.0090, 0.0095 and 0.018 min^{-1}, respectively.

In the presence of UV light, charge transfer presumably takes place from the HOMO of O and/or N atoms, to the LUMO, which is likely to be centered on the Mn atom [11, 41–43]. Excited state electrons in the LUMO are usually very easily lost, while the HOMO can readily accept an electron to return to its stable ground state [11]. Therefore, electrons are captured from water molecules to produce ·OH active species, which can destroy organic dyes such as MB efficiently in the photocatalytic process [43, 44].

In order to confirm the proposed mechanism, radical trapping experiments were carried out to detect the main oxidative species in these reactions [45]. The results revealed that the addition of 1 mM isopropanol (IPA) as a radical scavenger significantly inhibited the degradation efficiencies of MB (decreased from 91.9 to 40.9 %) under UV irradiation for 120 min, with k being 0.0046 min^{-1} (compared to 0.018 min^{-1} without IPA as radical trapping agent), as illustrated in Fig. 5. This is consistent with the involvement of ·OH radicals in the photodegradation reactions.

Conclusions

Three novel coordination compounds were synthesized by hydrothermal methods and characterized by X-ray diffraction analysis, as well as physico-chemical and spectroscopic analysis. Complex **1** consisted of 2D neutral sheets, while complex **2** had a 1D structure. The different dimensionalities can be attributed to the different O–Mn–O angles in these complexes, although the Mn(II) centers and the organic ligands adopted identical coordination modes. Complex **3** was a supramolecular 0D coordination complex. All three complexes exhibited photocatalytic activities to decompose MB under UV irradiation, believed to be mediated by ·OH radicals. Compared to those complexes already described in the literatures [11], complex **3** possesses average catalytic activities to degrade MB. Further research should be carried out to investigate their photocatalytic activities with respect to other organic pollutants.

Supplementary material

CCDC 1042969, 1042971 and 1042976 contain the supplementary crystallographic data for compounds **1**, **2** and **3**. These data can be obtained free of charge from The Cambridge Crystallographic Data Centre via www.ccdc.cam.ac.uk/data_request/cif.

Acknowledgments We thank the financial support from National Natural Science Foundation of China (51578034), the Beijing Natural Science Foundation & Scientific Research Key Program of Beijing Municipal Commission of Education (KZ201410016018, KM201510016017), the Training Program Foundation for the Beijing Municipal Excellent Talents (2013D005017000004), the Importation & Development of High-Caliber Talents Project of Beijing Municipal Institutions (CIT&CD201404076), and the R&D Base Project for the Synergic Innovation Centre of Energy Saving and Carbon Emission Reduction under the Jurisdiction of Beijing Municipality (2016).

References

1. Hasegawa S, Horike S, Matsuda R, Furukawa S, Mochizuki K, Kinoshita Y, Kitagawa S (2007) Three-dimensional porous coordination polymer functionalized with amide groups based on tridentate ligand: selective sorption and catalysis. J Am Chem Soc 129(9):2607–2614
2. Wen T, Zhang D-X, Liu J, Lin R, Zhang J (2013) A multifunctional helical Cu (I) coordination polymer with mechanochromic, sensing and photocatalytic properties. Chem Commun 49(50):5660–5662
3. Zhang Y-Q, Wang C-C, Zhu T, Wang P, Gao S-J (2015) Ultra-high uptake and selective adsorption of organic dyes with a novel polyoxomolybdate-based organic–inorganic hybrid compound. RSC Adv 5(57):45688–45692
4. Kuppler RJ, Timmons DJ, Fang Q-R, Li J-R, Makal TA, Young MD, Yuan D, Zhao D, Zhuang W, Zhou H-C (2009) Potential applications of metal–organic frameworks. Coord Chem Rev 253(23):3042–3066
5. Caskey SR, Wong-Foy AG, Matzger AJ (2008) Dramatic tuning of carbon dioxide uptake via metal substitution in a coordination polymer with cylindrical pores. J Am Chem Soc 130(33):10870–10871
6. Wang C-C, Li H-Y, Guo G-L, Wang P (2013) Synthesis, characterization, and luminescent properties of a series of silver (I) complexes with organic carboxylic acid and 1, 3-bis (4-pyridyl) propane ligands. Transit Met Chem 38(3):275–282
7. Wang C-C, Guo G-L, Wang P (2013) Synthesis, structure, and luminescent properties of three silver (I) complexes with organic carboxylic acid and 4, 4′-bipyridine-like ligands. Transit Met Chem 38(4):455–462
8. Ming C-L, Hao Z-C, Yu B-Y, Van Hecke K, Cui G-H (2015) Synthesis, structures, and catalytic properties of three new metal–organic coordination polymers constructed from flexible benzimidazole-Based and cis-1, 2-cyclohexanedicarboxylate synthons. J Inorg Organomet Polym Mater 25(3):559–568
9. Wang S, Wang X (2015) Multifunctional metal–organic frameworks for photocatalysis. Small 11:3097
10. Jing H-P, Wang C-C, Zhang Y-W, Wang P, Li R (2014) Photocatalytic degradation of methylene blue in ZIF-8. RSC Adv 4(97):54454–54462
11. Wang C-C, Li J-R, Lv X-L, Zhang Y-Q, Guo G (2014) Photocatalytic organic pollutants degradation in metal–organic frameworks. Energy Environ Sci 7(9):2831–2867
12. Wang C-C, Xu D-X, Jing H-P, Guo X-X, Wang P, Gao S-J (2015) Two zinc based coordination compounds constructed from two azophenyl ligands: syntheses, crystal structure, and photocatalytic performance. J Inorg Organomet Polym Mater 26(1):276–284
13. Wang C-C, Zhang Y-Q, Li J, Wang P (2015) Photocatalytic CO_2 reduction in metal–organic frameworks: a mini review. J Mol Struct 1083:127–136
14. Fu Y, Sun D, Chen Y, Huang R, Ding Z, Fu X, Li Z (2012) An amine-functionalized titanium metal–organic framework photocatalyst with visible-light-induced activity for CO_2 reduction. Angew Chem 124(14):3420–3423
15. Lin H, Maggard PA (2008) Synthesis and structures of a new series of silver-vanadate hybrid solids and their optical and photocatalytic properties. Inorg Chem 47(18):8044–8052
16. Toyao T, Saito M, Horiuchi Y, Mochizuki K, Iwata M, Higashimura H, Matsuoka M (2013) Efficient hydrogen production and photocatalytic reduction of nitrobenzene over visible-light-responsive metal–organic framework photocatalyst. Catal Sci Technol 3(8):2092–2097
17. Wang C-C, Zhang Y-Q, Zhu T, Zhang X-Y, Wang P, Gao S-J (2015) Four coordination compounds constructed from 1, 10-phenanthroline and semi-flexible and flexible carboxylic acids: hydrothermal synthesis, optical properties and photocatalytic performance. Polyhedron 90:58–68
18. Wang C-C, Wang P, Guo G-L (2012) 3D sandwich-like frameworks constructed from silver chains: synthesis and crystal structures of six silver (I) coordination complexes. Transit Met Chem 37(4):345–359
19. Zhang J, Wang C-C, Wang P, Gao S-J (2015) Three silver complexes constructed from organic carboxylic acid and 1,2-bis(4-pyridyl)ethane ligands: syntheses, crystal structures and luminescent properties. Transit Met Chem 40(8):821–829
20. Wang C, Jing H, Wang P, Gao S (2015) Series metal–organic frameworks constructed from 1,10-phenanthroline and 3,3′,4,4′-biphenyltetracarboxylic acid: hydrothermal synthesis, luminescence and photocatalytic properties. J Mol Struct 1080:44–51
21. Ye B-H, Tong M-L, Chen X-M (2005) Metal–organic molecular architectures with 2, 2′-bipyridyl-like and carboxylate ligands. Coord Chem Rev 249(5):545–565
22. Zou H-H, Yin X-H, Sun X-J, Zhou Y-L, Hu S, Zeng M-H (2010) A unique 2D framework containing rhombic tetrameric cobalt(II) of mixed Td and Oh geometries linked by two different rigid ligands: synthesis, crystal structure and magnetic properties. Inorg Chem Commun 13(1):42–45
23. Liu G, Zhou H, Ren X (2011) Synthesis, structure and near-infrared luminescence of a new 2D praseodymium(III) coordination polymer. J Rare Earths 29(11):1100–1104
24. Wang X-F, Yu M, Liu G-X (2015) A series of coordination polymers based on varied polycarboxylates and different imidazole-containing ligands: syntheses, crystal structures and physical properties. RSC Adv 5(98):80457–80471
25. Reinsch H, Waitschat S, Stock N (2013) Mixed-linker MOFs with CAU-10 structure: synthesis and gas sorption characteristics. Dalton Trans 42(14):4840–4847
26. Chang X-H, Ma L-F, Hui G, Wang L-Y (2012) Four low-dimensional cobalt(II) coordination polymers based on a new isophthalic acid derivative: syntheses, crystal structures, and properties. Cryst Growth Des 12(7):3638–3646
27. Bruker AXS SMART, Version 5.611, Bruker AXS, Madison, WI, USA (2000)
28. SADABS V2.03, Bruker AXS, Madison, WI (2000)
29. Sheldrick GM SHELX-97, GÖttingen University, Germany (1997)
30. Ma L-F, Li X-Q, Meng Q-L, Wang L-Y, Du M, Hou H-W (2010) Significant positional isomeric effect on structural assemblies of Zn (II) and Cd (II) coordination polymers based on bromoisophthalic acids and various dipyridyl-type coligands. Cryst Growth Des 11(1):175–184
31. Liu G-X, Huang R-Y, Xu H, Kong X-J, Huang L-F, Zhu K, Ren X-M (2008) Controlled assembly of zero-, one-and two-dimensional metal–organic frameworks involving in situ ligand synthesis under different reaction pH. Polyhedron 27(11):2327–2336
32. Liu J-Q (2011) Syntheses and structural characterization of two metal–organic frameworks from tripodal and dipodal ligands. J Coord Chem 64(10):1807–1814
33. Jia J, Athwal HS, Blake AJ, Champness NR, Hubberstey P, Schröder M (2011) Increasing nuclearity of secondary building units in porous cobalt (ii) metal–organic frameworks: variation in structure and H 2 adsorption. Dalton Trans 40(45):12342–12349
34. Ma L-F, Li X-Q, Wang L-Y, Hou H-W (2011) Syntheses and characterization of nickel(II) and cobalt(II) coordination polymers based on 5-bromoisophthalate anion and bis (imidazole) ligands. CrystEngComm 13(14):4625–4634
35. Patra R, Titi HM, Goldberg I (2013) Crystal engineering of molecular networks: tailoring hydrogen-bonding self-assembly of

tin-tetrapyridylporphyrins with multidentate carboxylic acids as axial ligands. Cryst Growth Des 13(3):1342–1349
36. Wang C-C, Jing H-P, Zhang Y-Q, Wang P, Gao S-J (2015) Three coordination compounds of cobalt with organic carboxylic acids and 1,10-phenanthroline as ligands: syntheses, structures and photocatalytic properties. Transit Met Chem 40(5):573–584
37. Shi D, Wang Z, Xing J, Li Y, Luo J, Chen L, Zhao J (2012) A 2-D organic–inorganic hybrid copper-yttrium heterometallic monovacant keggin phosphotungstate derivative: [Cu(-dap)2]5.5[Y(α-PW11O39)2]·4H_2O. Synth React Inorg Met-Org Nano-Met Chem 42(1):30–36
38. Du P, Yang Y, Yang J, Liu B-K, Ma J-F (2013) Syntheses, structures, photoluminescence, photocatalysis, and photoelectronic effects of 3D mixed high-connected metal–organic frameworks based on octanuclear and dodecanuclear secondary building units. Dalton Trans 42(5):1567–1580
39. Stylianou KC, Heck R, Chong SY, Bacsa J, Jones JT, Khimyak YZ, Bradshaw D, Rosseinsky MJ (2010) A guest-responsive fluorescent 3D microporous metal–organic framework derived from a long-lifetime pyrene core. J Am Chem Soc 132(12):4119–4130
40. Laurier KG, Vermoortele F, Ameloot R, De Vos DE, Hofkens J, Roeffaers MB (2013) Iron (III)-based metal–organic frameworks as visible light photocatalysts. J Am Chem Soc 135(39): 14488–14491
41. Nasalevich M, Van der Veen M, Kapteijn F, Gascon J (2014) Metal–organic frameworks as heterogeneous photocatalysts: advantages and challenges. CrystEngComm 16(23):4919–4926
42. Lopez HA, Dhakshinamoorthy A, Ferrer B, Atienzar P, Alvaro M, Garcia H (2011) photochemical response of commercial MOFs: Al2 (BDC) 3 and its use as active material in photovoltaic devices. J Phys Chem C 115(45):22200–22206
43. Mahata P, Madras G, Natarajan S (2006) Novel photocatalysts for the decomposition of organic dyes based on metal–organic framework compounds. J Phys Chem B 110(28):13759–13768
44. Yu ZT, Liao ZL, Jiang YS, Li GH, Chen JS (2005) Water-insoluble Ag–U–organic assemblies with photocatalytic activity. Chem Eur J 11(9):2642–2650
45. Zhang H, Zong R, Zhao J, Zhu Y (2008) Dramatic visible photocatalytic degradation performances due to synergetic effect of TiO2 with PANI. Environ Sci Technol 42(10):3803–3807